UDC669.184.2:621.746

Advances in Technology of Oxide Metallurgy

Shigeaki Ogibayashi*1

Abstract:

Nonmetallic inclusions are generally considered harmful, and assiduous studies have been made to remove them. If their properties are positively controlled and utilized, however, they should lead to an improvement in steel quality and development of new functional materials. From this point of view, Nippon Steel has engaged in the development of oxide metallurgy, which is a new concept of utilizing oxides as precipitate nucleation sites. This paper generally describes the basic concept of oxide metallurgy, oxide control methods in the steelmaking process, and examples of industrial application of oxide metallurgy to improvements in the properties of titanium-deoxidized steel with high HAZ toughness for plates, and of high-toughness hot-forging microalloyed steel for machine structural use. Also presented is the future outlook of oxide metallurgy.

1. Introduction

Nonmetallic inclusions often cause surface and internal defects in steel products. They have been considered harmful to steel, and various techniques have been developed to remove them. Many of such harmful inclusions are 50 μm or larger in size in the as-cast steel. On the other hand, small oxides measuring several micrometers or less in size serve as precipitation sites for sulfides and carbonitrides in the solidification and rolling stages. Steel properties can be drastically improved by judiciously controlling the dispersion, composition, and size of small oxides. Nippon Steel coined the term "oxide metallurgy" for the technology of controlling the fine dispersion and composition of oxides[1], and has applied the technology to the improvement of steel properties and development of new steel products. Here are described the basic concept of oxide metallurgy, technology of controlling oxides in the steelmaking process, and the application of oxide metallurgy to the improvement of steel properties.

2. Basic Concept of Oxide Metallurgy

It is well-known that precipitates of sulfides and carbonitrides, for instance, have a great influence on the properties of steel. Since these precipitates normally precipitate at grain boundaries and sites of high dislocation density, steel properties are generally controlled through grain refinement and work dislocation through hot rolling and controlled cooling. On the other hand, since these precipitates are generally considered to nucleate from heterogeneous phases such as oxides, various steel properties are considered controllable by uniformly dispersing oxides in the steel and thereby dispersing many precipitates with the dispersed oxides as nuclei after solidification of the steel[1]. To confirm this relationship, the relationship between the locations of MnS precipitates and oxides was investigated respectively for vacuum melted steel and oxygen-bearing Mn-Si-Zr killed steel by a computer-aided electron probe microanalyzer (CMA)[2]. As a result, it was found that MnS is distributed only in the microsegregation of manganese in the case of vacuum melted steel with an oxygen concentration of 9 ppm or less in which few or no oxides are present, while in the case of Mn-Si-Zr killed steel, MnS is finely dispersed on oxides.

Photo 1 shows an example of intra-granular ferrite precipitated on MnS[3,4]. This intra-granular ferrite was observed in the Mn-Si-Al killed steel which was subjected to heat treatment at 1,300°C and cooled at 0.1 to 0.3°C/s. It is evident that MnS precipitated on a $MnO\text{-}Al_2O_3$ complex oxide and that intra-

*1 Technical Development Bureau

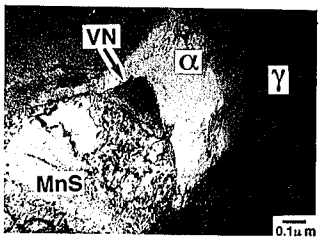

(a) Intra-granular ferrite formed in VN precipitates on MnS

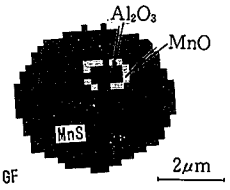

(b) Electron reflection map of cross section through MnS

Photo 1 Intra-granular ferrite formed in VN and MnS precipitates on $MnO-Al_2O_3$ oxide

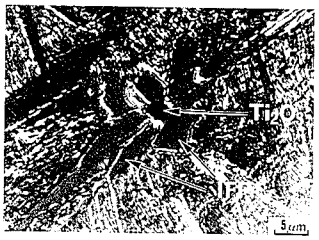

(a) Nucleation of intra-granular ferrite from Ti_2O_3

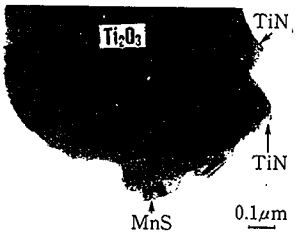

(b) Precipitation of MnS and TiN on Ti_2O_3

Photo 2 Intra-granular ferrite formed in Ti_2O_3 accompanying MnS and TiN

granular ferrite precipitated from VN as nucleus precipitated on MnS. **Photo 2** shows an example of intra-granular ferrite precipitated on Ti_2O_3[1,5]. This intra-granular ferrite was observed in the titanium-deoxidized steel specimen which was cooled from the austenite region. A closer examination reveals that the oxide is a Ti_2O_3 complex oxide and that MnS and TiN precipitate on the Ti_2O_3 complex oxide.

The technology of controlling the properties of steel by utilizing fine oxides in the steel as nuclei for precipitation as seen in these examples is called oxide metallurgy and applied to the development of various new steel products. Takamura et al.[1] report that MnS and other precipitates are likely to precipitate on oxides of the cation vacancy type and that oxides of the anion vacancy type do not readily serve as sites for precipitation. Precipitation of MnS depends on oxide melting point and sulfide capacity, as described later. To utilize oxides as nucleation sites for precipitation, the oxides must be finely dispersed and their composition be properly controlled.

Fig. 1 shows the basic concept of oxide metallurgy. As shown, the properties of steel with a small hot working ratio and of weldable steel, for example, can be improved through the inhibition of grain growth by the pinning action of precipitates and through grain refinement by the formation of intra-granular ferrite. In the steelmaking process, the key technology for controlling the melting point of oxides in order to control their deformability, is basically the same as that for controlling them as nucleation sites for precipitation. We call these technologies as a whole by a generic term "oxide metallurgy".

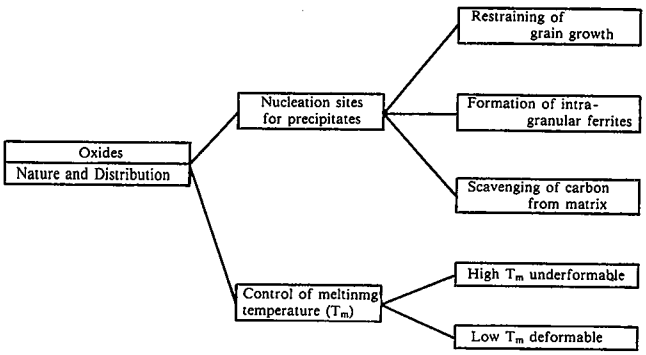

Fig. 1 Basic concept of oxide metallurgy for steel

3. MnS Precipitation Control Technology

3.1 Effect of oxide composition on MnS precipitation[6,7]

Fig. 2 shows the effects of the type of deoxidizing element and sulfur on the precipitation ratio of MnS on oxides as investigated by 1-kg steel melting experiment[2,6]. When the steel is deoxidized by aluminum or zirconium, the oxide is Al_2O_3 or ZrO_2, respectively, and the MnS precipitation ratio steeply decreases with decreasing sulfur concentration when the latter is less than 100 ppm. When the steel is deoxidized by manganese and silicon, on the other hand, the MnS precipitation ratio is held high even if the sulfur concentration is low. When the steel is deoxidized by manganese and titanium, the MnS precipitation ratio falls between the above two cases. In summary, when the sulfur concentration is more than 100 ppm, MnS precipitates as nuclei for most of oxides present in the steel, irrespective of the type of oxide. When it is less than 100 ppm, the MnS precipitation heavily depends on the type of oxide.

Fig. 3 compares the MnS precipitation ratio and the MnS solu-

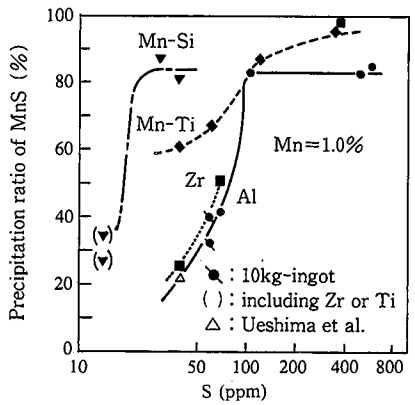

Fig. 2 Change in precipitation ratio of MnS on oxides with sulfur concentration and type of deoxidizing element[2,6]

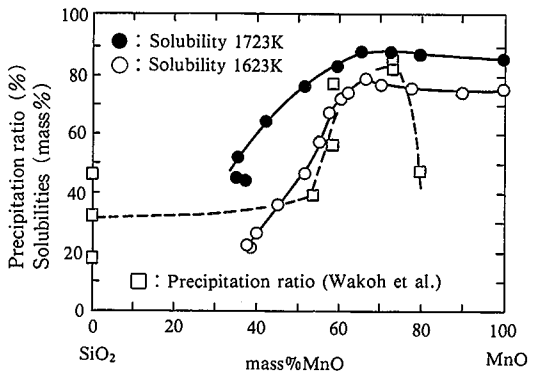

Fig. 3 Precipitation ratio and solubility of MnS in molten $MnO-SiO_2$ system[8]

bility of manganese silicate in the $MnO\text{-}SiO_2$ system[8]. The two variables agree well in tendency. The precipitation ratio of MnS steeply increases when MnO is 40% or more and peaks when MnO is 60% or more. When MnO exceeds 80%, the precipitation ratio of MnS becomes lower although the solubility of MnS keeps high, because the oxides solidify in the molten steel as their melting point exceeds 1,600°C.

From the above results, the mechanism of the MnS precipitation may be interpreted as follows[7]:

(1) When the oxide of interest is solid in the molten steel, MnS precipitates on the surface of the oxide because of the decreasing solubility of MnS with decreasing temperature after the solidification of steel and grows with the diffusion of manganese and sulfur from the steel matrix. With this mechanism, the precipitation ratio of MnS depends on the sulfur concentration and steeply decreases with decreasing sulfur concentration when the latter is less than 100 ppm.

(2) When the oxide of interest is liquid in the molten steel, sulfur, dissolved in the oxide because of the distribution between the molten steel and the oxide, crystallizes as MnS on the oxide surface because of temperature drop after the solidification of steel and because of a decrease in the solubility of MnS with the solidification of the molten oxide. This initial crystallization of MnS triggers the subsequent precipitation of MnS in the lower temperature region. When the solubility of MnS in the oxide is high, the manganese and sulfur dissolve as MnS in the oxide after the solidification of steel. The above mechanism is thus promoted further, and the precipitation ratio of MnS is maintained high when the sulfur concentration ratio is less than 100 ppm.

According to the above-mentioned mechanism, when the sulfur concentration is more than 100 ppm, the precipitation of MnS depends little on the type of oxide, and the fine dispersion of MnS needs the fine dispersion of the oxide concerned. When the sulfur concentration is less than 100 ppm, the oxide must be controlled to a composition with a low melting point and high sulfide capacity, in addition to the fine dispersion of the oxide.

4. Oxide Control Technology

If oxides are to be utilized as nucleation sites for the precipitation of MnS, they must be of such composition as to provide many nuclei for the MnS precipitation and must be finely dispersed in large amounts. When aluminum, a strong deoxidizing element, is added in large amounts to steel, the resultant oxide composition is single Al_2O_3. Since the free oxygen concentration before the solidification of steel is also low, the change in the oxide composition during the solidification is practically ignorable, and oxide control is relatively easy to perform. High-melting-point oxides such as Al_2O_3 are disadvantageous in that they cannot readily become nucleation sites for the precipitation of MnS. Complex deoxidation in combination with strong deoxidizing elements as shown in **Fig. 4** is effective in dispersing many complex oxides as nucleation sites for the precipitation of MnS. In this case, it is important that strong deoxidizing elements should be added in appropriate amounts to form such complex oxides that facilitate the precipitation of MnS.

Fig. 5 shows the change of oxide composition with the addition of strong deoxidizing elements as investigated by laboratory experiments[9]. The number of manganese silicate oxides decreases with increasing zirconium addition, and the number

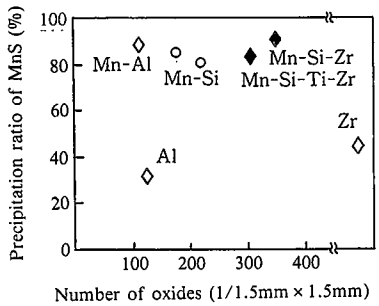

Fig. 4 Effect of deoxidizing elements on precipitation ratio of MnS and number of oxides[7]

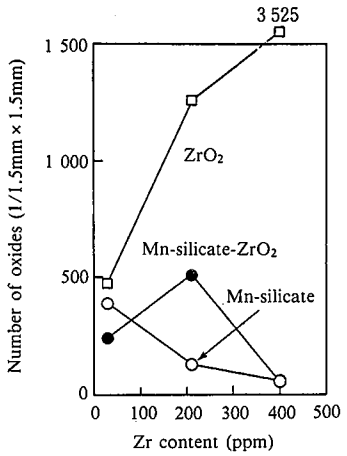

Fig. 5 Change in number of oxide particles with addition of zirconium[9]

of Mn-Si-Zr complex oxides is maximum when the zirconium content is 200 ppm. **Fig. 6** shows the calculated oxide composition under the experimental conditions as thermodynamically analyzed by a mathematical model[10] formulated by applying SOLGAXMIX[11] developed by Eriksson et al. The algorithm of thermodynamic equilibrium computation is shown in **Fig. 7**[10]. The calculated values agree well with the measured values shown in **Fig. 5**. Various complex deoxidation systems, including the Mn-Si-Ti-Zr and Mn-Si-Ca-Al systems, can be similarly analyzed. The equilibrium of molten steel and oxides in such multicomponent systems was virtually impossible to analyze in the past, but now can be quantitatively predicted by the above mathematical model[10,12]. In the manganese-silicon-deoxidized steel without strong deoxidizing elements, the effects of ladle slag and refractories cannot be ignored for predicting the oxide composition. The mathematical model can quantitatively predict the oxide composition in molten steel by taking into account the partial equilibrium of molten steel with ladle slag and refractories, and is applied in the industrial deoxidation control of molten steel.

In complex deoxidation systems that contain only trace amounts of strong deoxidizing elements, the free oxygen content before solidification is relatively high. As the formation and compositional change of oxides during solidification have a large influence, the number and composition of oxides depend on the cooling rate during solidification. Typical examples are given in **Figs. 8** and **9**[13,14]. In titanium-deoxidized steel that is weakly deoxidized compared with the aluminum-calcium-deoxidized steel to which are added strong deoxidizing elements in large amounts, the number of oxides increases with increasing cooling rate, the

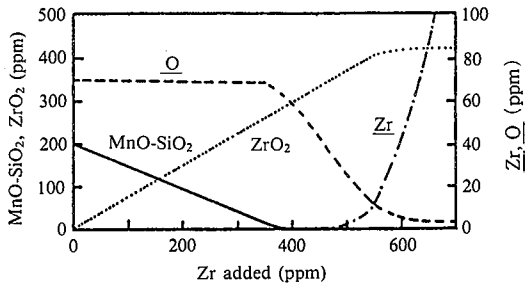

Fig. 6 Results of calculation by SOLGASMIX concerning formation of oxides[9]

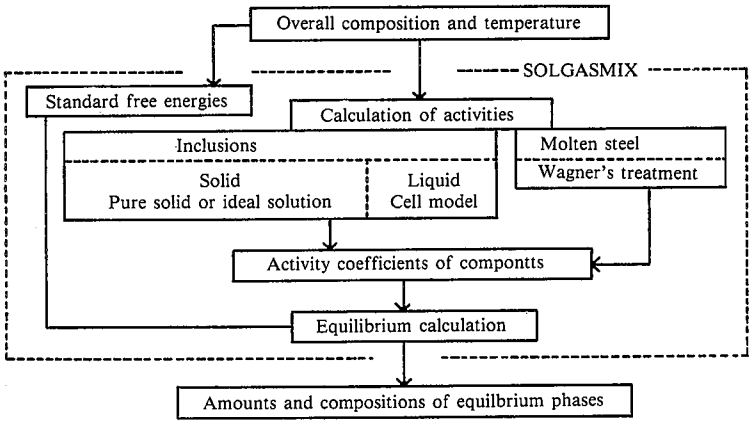

Fig. 7 Calculation algorithm for equilibrium state between molten steel and nonmetallic inclusions[10]

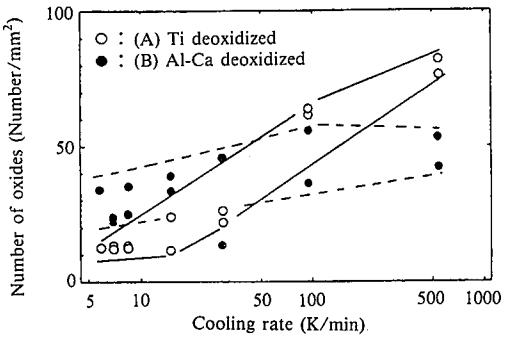

(A) 0.06C-0.05Si-1.20Mn-0.001Al-0.014Ti-0.0027O
(B) 0.04C-0.26Si-1.26Mn-0.037Al-0.0020Ca-0.0019O

Fig. 8 Change in number of oxides with cooling rate in titanium-deoxidized steel and aluminum-calcium-deoxidized steel[13]

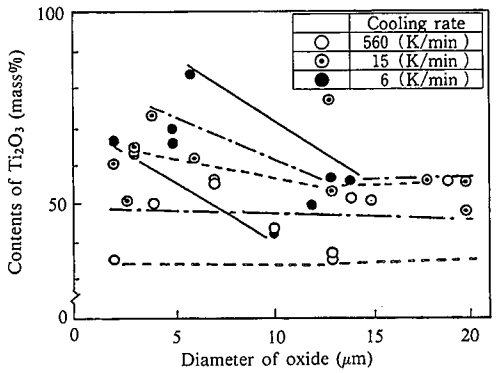

Fig. 9 Relationship between content of Ti_2O_3 and particle size of oxides in titanium-deoxidized steel[14]

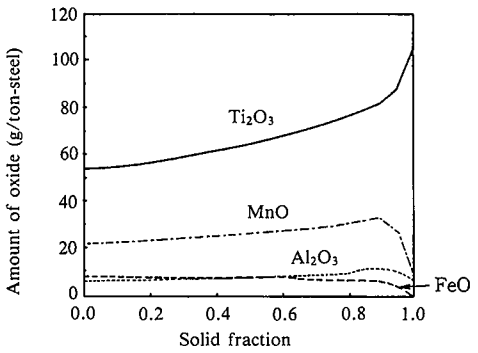

Fig. 10 Calculation by equilibrium model of change in chemical composition of oxides in titanium-deoxidized steel during solidification[14]

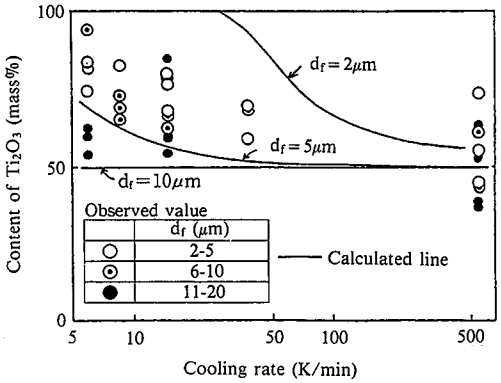

Fig. 11 Changes in calculated and measured contents of Ti_2O_3 with cooling rate[14] (d_f: oxide particle size at end of solidification)

composition of oxides depends on the cooling rate and oxide particle size, and the change of oxide composition during solidification increases with decreasing cooling rate and oxide particle size.

This change in oxide composition during solidification can be quantitatively explained by equilibrium analysis between molten steel and oxides that allows for micro segregation during solidification and oxide entrapment into the solid phase[10,12]. The particle size dependence of oxide composition can be analyzed by taking into account the degree of supersaturation during solidification and the diffusion growth of oxides in the above-mentioned model[14]. **Fig. 10**[14] shows an example of analysis of the change of oxide composition in the titanium-deoxidized steel during solidification. Calculated and observed oxide compositions as a function of cooling rates for various oxide particle sizes are shown in **Fig. 11**[14]. When the oxide particle size is small, the Ti_2O_3 concentration steeply increases with decreasing cooling rate. When the oxide particle size is large, the particle size dependence of Ti_2O_3 decreases. The calculated values agree fairly well with the observed values.

As discussed above, the formation of deoxidization products during solidification has a large effect in weak deoxidation systems. The number and composition of oxides are strongly influenced by the cooling rate. As a result, the particle size distribution of oxides is also strongly influenced by the cooling rate during solidification. **Fig. 12** shows the effect of the cooling rate during solidification on the particle size distribution of fine oxides in the titanium-deoxidized steel and calcium-aluminum-deoxidized steel[12]. In the calcium-aluminum-deoxidized steel, the particle size distribution of oxides depends little on the cool-

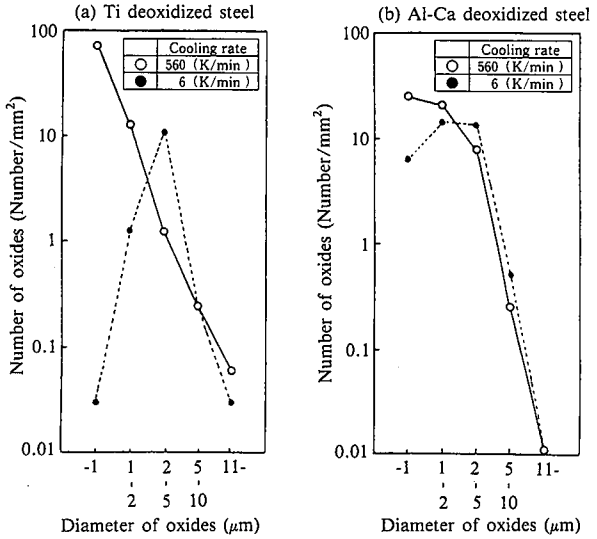

Fig. 12 Comparison of cooling rate and oxide particle size distribution in titanium-deoxidized steel (a) and aluminum-calcium-deoxidized steel (b)[13]

ing rate during solidification. In the titanium-deoxidized steel, the cooling rate during solidification has a large influence on the particle size distribution of oxides. When the cooling rate is high, many fine oxides of 1 μm or less in size form during solidification.

When the cooling rate is low, on the other hand, oxides 2 to 3 μm in size account a majority of oxides. This is because decreasing the cooling rate prolongs the diffusion time of elements comprising the products of secondary deoxidation and accelerates the growth of oxides during solidification. This can be analyzed by the above-mentioned model. This result indicates that secondary deoxidation in a weakly deoxidized steel can be effectively utilized for the fine dispersion of oxides, and that complex deoxidation through the combined use of strong deoxidizing elements in trace amounts is effective in increasing the number of fine oxides.

As described above, the formation of secondary deoxidation products is influenced by the cooling rate during solidification, and their behavior is complicated. The composition of oxides formed in various deoxidation systems can now be predicted by analytical models that analyze the equilibrium between the molten steel and oxides and take into consideration the degree of supersaturation and the diffusion growth of oxides. Oxides that can become nucleation sites for MnS, TiN, VN and other precipitates necessary for steel property control can be finely dispersed by appropriately selecting the additions of weak and strong deoxidizing agents to meet specific steel grades and properties.

5. Application to Steel Property Control

5.1 High-HAZ toughness titanium-deoxidized steel for plate

Generally in the heat-affected zone (HAZ) of low-carbon steel, the rolled structure is destroyed by reheating during welding, and coarse ferrite grows from prior austenite grain boundaries during cooling after welding and markedly deteriorates the low-temperature toughness. The HAZ toughness of low-carbon steel can be significantly improved by intentionally forming intragranular ferrite precipitating at oxide and sulfide particles used as transformation nuclei in the application of oxide metallurgy.

This type of steel is called titanium-deoxidized steel and is commercially produced. The typical chemical composition of the titanium-deoxidized steel is given in **Table 1**[15]. The titanium-deoxidized steel is characterized by appropriate contents of titanium and nitrogen and a very low aluminum content of about 20 ppm.

Fig. 13 shows the effect of aluminum on the Ti_2O_3 concentration in the Ti_2O_3-Al_2O_3-MnO complex oxide[15]. Since the Ti_2O_3 concentration rapidly diminishes as the aluminum content exceeds 30 ppm, the aluminum content must be controlled at low levels. Titanium is added in the secondary refining stage. **Photo 3** shows the crystal structure of a simulated HAZ as obtained in the weld heat cycle test[15]. Fine acicular ferrite is formed throughout the specimen, and titanium oxide particles are observed as nuclei for the fine acicular ferrite. X-ray analysis identified the titanium oxide as Ti_2O_3. As shown in **Photo 2**, it is a complex Ti-Mn oxide on which MnS and TiN precipitate. Various mechanisms are proposed for complex oxides serving as transformation nuclei for ferrite. The largest governing factor appears to be crystal lattice coherency between precipitates and ferrite[3]. As other influencing factors for the Ti_2O_3 steel, Ti_2O_3 particles contain cation vacancies, and manganese is absorbed by Ti_2O_3 particles because of the valence electron number balance between the cation vacancies and oxygen, and a manganese-depleted layer is likely to form around each oxide[5,16]. These are also considered to affect the complex oxides that serve as ferrite transfor-

Table 1 Example of chemical composition of titanium-deoxidized steel

C	Si	Mn	P	S	Cu	Ni	Nb	Al	Ti	N
0.082	0.17	1.54	0.004	0.002	0.22	0.24	0.013	0.003	0.014	0.0020

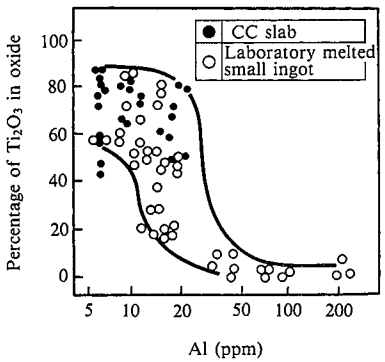

Fig. 13 Effect of aluminum content on oxide composition[15]

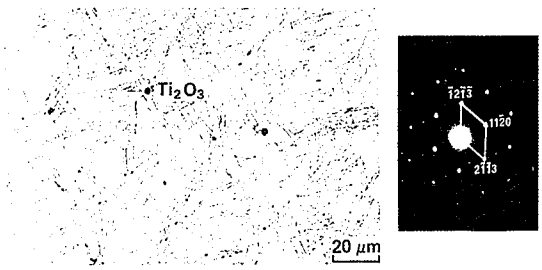

Photo 3 Intra-granular ferrite nucleated from titanium deoxidation product particles in specimen rapidly cooled from 600°C in weld heat cycle test[15]

mation nuclei.

Fig. 14 shows the relationship between the number of titanium oxide particles and the volume fraction of intra-granular ferrite. **Fig. 15**[15] shows the relationship between the volume fraction of intra-granular ferrite and the transition temperature in Charpy V-notch impact test. The volume fraction of intra-granular ferrite sharply increases with increasing titanium oxide particles at a level of 5 to 10 per mm^2 or more, which in turn lowers the transition temperature and improves the low-temperature toughness.

Fig. 16[15] shows the Charpy V-notch transition temperature when the peak temperature is changed in the high-heat input weld simulation test. The transition temperature increases with increasing welding heat input for the TiN steel, but changes little with welding heat input for the Ti_2O_3 steel. With the TiN steel, TiN decomposes and dissolves in the steel at 1,350°C. With the titanium-deoxidized steel, MnS and TiN, precipitated from oxide nuclei, decompose at the high temperature of welding but precipitate again from stable oxide particles during cooling. Accordingly approximately the same precipitate distribution as obtained before welding is obtained again. **Fig. 17**[15] shows the relationship between the CTOD value and welding heat input, as compared with the TiN steel. Stable CTOD values are secured at high heat input for the Ti_2O_3 steel. This is an outstanding feature of the Ti_2O_3 steel. The CTOD value of the TiN steel steeply decreases with increasing heat input, because a brittle region is locally present near the fusion line. The Ti_2O_3 steel has CTOD values much superior to those of the TiN steel, thanks to the grain refinement of the HAZ structure near the fusion line that can be controlled in the Ti_2O_3 steel but not in the TiN steel.

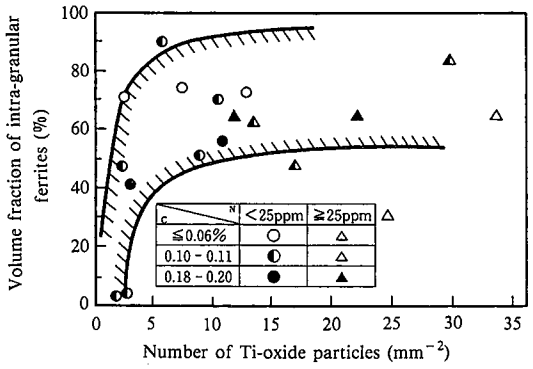

Steel composition: 0.05-0.19%C, 0.2%Si, 1.38-1.4%Mn, 0.0004-0.0008%S, 0.012-0.018%:Ti, 0.01-0.022%sol.Al, 0.0007-0.0046%N

Fig. 14 Relationship between number of titanium oxide particles and volume fraction of intra-granular ferrite in simulated HAZ[15]

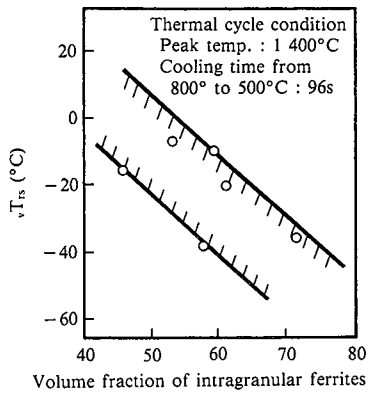

Steel composition: 0.08%C-1.5%Mn-0.013%Nb-0.003%Al-0.012%Ti-0.0023%N

Fig. 15 Relationship between Charpy V-notch impact transition temperature and volume fraction of intra-granular ferrite in simulated HAZ[15]

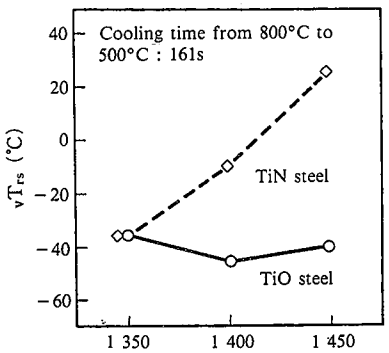

Chemicalk composition (wt%)

Steel	C	Si	Mn	P	S	Al	Ti	N
TiO	0.08	0.20	1.4	0.01	0.001	0.002	0.012	0.0020
TiN	0.08	0.20	1.4	0.01	0.001	0.020	0.018	0.0050

Fig. 16 Change in Charpy V-notch impact transition temperature of simulated HAZ with peak temperature[15]

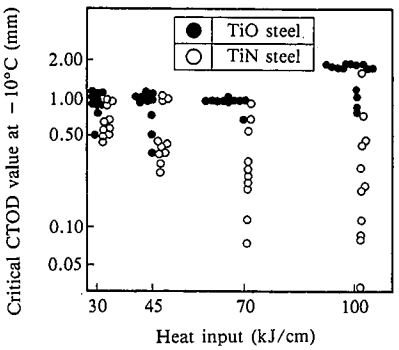

Fig. 17 Critical CTOD value versus heat input

5.2 High-toughness hot-forging microalloyed steel for machine structural use

Hot-forging steels, generally used in component parts of machines such as automobiles and industrial machines, are forged, quenched and tempered to produce the desired toughness. If fine intra-granular ferrite is nucleated from MnS, high toughness can be obtained without quenching and tempering. **Table 2**[17] gives the chemical composition of a hot-forging steel developed for use without quenching and tempering, through the application of oxide metallurgy. The steel is a 0.25%C aluminum-killed grade containing vanadium, sulfur, and nitrogen. **Photo 4** shows the microstructures of specimens cooled at a rate of 0.1 K/s from 1,523K[17]. When no vanadium is added, there are observed a coarse ferrite structure formed from prior austenite grain boundaries and a pearlite structure enclosed by the coarse ferrite structure. The 0.13%V-0.021%N steel exhibits a massive formation of fine intra-granular ferrite, thanks to the vanadium nitrides, which have a good lattice coherency with ferrites precipitated on manganese sulfides on oxides.

Table 2 Chemical composition of V-N bearing steel (example)

(mass %)

C	Si	Mn	P	S	Cr	V	Al	Ti	N
0.25	0.38	1.54	0.012	0.070	0.25	0.13	0.035	<0.002	0.015

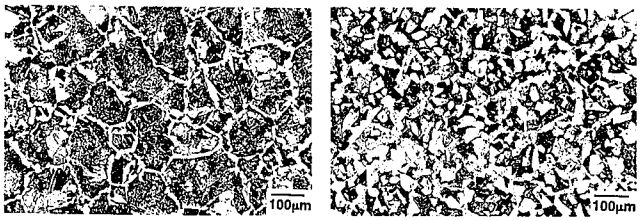

(a) V-free 0.023%N steel (b) 0.13%V-0.021%N steel

Photo 4 Effects of vanadium and nitrogen contents on microstructure[17]

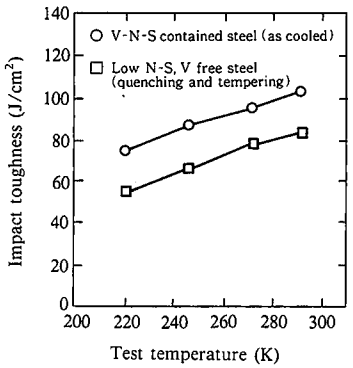

Fig. 18 Impact toughness of hot-forging microalloyed steel[17]

The effects of sulfur and nitrogen on the ferrite-pearlite structure of the vanadium-nitrogen-microalloyed steel were also investigated[18]. Increasing the sulfur and nitrogen contents was found to reduce the grain size of the austenite structure, precipitate many fine ferrite particles in the austenite grains, and refine the structure. This austenite grain refinement can be attributed to the pinning effect of grain boundaries by MnS and VN in the temperature region below 1,100°C, and mainly to MnS in the hot-forging temperature region of 1,250°C. MnS is thus has the effects of both nucleating intra-granular transformation and inhibiting the grain coarsening of austenite during hot forging.

Fig. 18 shows the Charpy V-notch impact toughness of the 0.13%V-0.015%N-0.07%S steel as compared with the conventional steel without vanadium and nitrogen additions[17]. The impact toughness of the 0.13%V-0.15%N-0.07%S steel is better than that of the conventional quenched and tempered steel.

5.3 Application to other steel grades

The idea of controlling steel properties by utilizing oxides as precipitate nucleation sites can be applied to a wide range of steel products. Besides the plate and hot-forging steels discussed above, Nippon Steel is pushing ahead with the development of new steel products through the application of oxide metallurgy to other steel grades, such as bars, shapes, rails, and electrical steel. Chemical composition control technology to control the deformability of oxides is applied to piano wire and stainless steel, with the result that a material with excellent drawing performance can be efficiently produced with stable quality.

6. Conclusions

The basic concepts of oxide metallurgy, technology for controlling oxides and MnS in the steelmaking process, and examples of its application to steel property control have been described. Oxide metallurgy is a completely new idea in that oxides are utilized as precipitate nucleation sites, and is applicable in principle to all steel grades. Nippon Steel is developing new steel products by applying oxide metallurgy to various steel product series. Oxide metallurgy is expected to expand its territory through the utilization of oxides as cementite precipitation sites, its application to the rapid solidification process and to the control of precipitates other than carbides and carbonitrides, and through further clarification of the sequence relationship between oxides and precipitates.

References

1) Takamura, J., Mizoguchi, S.: Proc. Sixth Int. Iron and Steel Congress. 1. 1990, p.591
2) Wakoh, M., Sawai, T., Mizoguchi, S.: Tetsu-to-Hagané. 78 (11), 1967 (1992)
3) Ishikawa, F., Takahashi, M., Enomoto, M.: Collected Abstracts of Japan Institute of Metals. October 1990, p.109
4) Koyasu, Y., Kanisawa, H., Ochi, T., Yanase, M., Takada, H., Naito, K., Ishikawa, F.: Shinnittetsu Giho. (343), 30 (1992)
5) Yamamoto, K., Aihara, S., Okamoto, K., Funaki, S.: CAMP-ISIJ. 3, 808 (1990)
6) Wakoh, M., Mizoguchi, S., Ogibayashi, S.: CAMP-ISIJ. 6, 252 (1993)
7) Wakoh, M.: Tohoku University thesis for degree. February 1993
8) Koyama, T., Dub, A.V., Tsukihashi, F., Sano, N.: CAMP-ISIJ. 5, 997 (1992)
9) Sawai, T., Wakoh, M., Ueshima, Y., Mizoguchi, S.: Proc. Sixth Int. Iron and Steel Congress. 1. 1990, p.605
10) Yamada, W., Matsumiya, T.: Proc. Sixth Int. Iron and Steel Congress. 1. 1990, p.618
11) Errikson, G.: Acta Chem. Scand. 25, 2651 (1971)
12) Yamada, W., Matsumiya, T.: Shinnittetsu Giho. (342), 38 (1991)
13) Goto, H., Miyazawa, K., Yamaguchi, K., Ogibayashi, S., Tanaka, K.: Tetsu-to-Hagané. 79 (9), 1082 (1993)
14) Goto, H., Miyazawa, K., Yamada, W., Tanaka, A.: Tetsu-to-Hagané. 80 (2), 113 (1994)
15) Chijiiwa, R., Tamehiro, H., Hirai, M., Matsuda, H., Mimura, H.: Proc. 7th Int. Conf. Offshore Mech. Arc. Eng. Vol. 5. 1988, p.165
16) Yamamoto, K., Hasegawa, T., Takamura, J.: Tetsu-to-Hagané. 79, 1169 (1993)
17) Ochi, T., Takahashi, T., Takada, N.: Iron & Steelmaker. 16 (2), 21 (1989)
18) Koyasu, Y., Takada, H., Takahashi, T., Takeda, H., Ishii, N.: Seitetsu Kenkyu. (337), 41 (1990)